

Dispersion of edge states and quantum confinement of electrons in graphene channels drawn on graphene fluoride

Ning Shen¹ and Jorge O. Sofo^{1,2,*}

¹*Department of Physics, The Pennsylvania State University, University Park, Pennsylvania 16802, USA*

²*Materials Research Institute, The Pennsylvania State University, University Park, Pennsylvania 16802, USA*

(Received 15 August 2010; revised manuscript received 7 January 2011; published 24 June 2011)

Graphene is an excellent conductor, while graphene fluoride is a wide band-gap semiconductor. We propose the formation of graphene channels embedded in graphene fluoride as a method to induce quantum confinement of charge carriers in graphene. In particular, we study the electronic structure of graphene channels drawn on the fluoride along two high-symmetry directions: the armchair and zigzag orientations. The zigzag channels are found to have dispersive one-dimensional edge bands, contrary to the case of ribbons and channels drawn on graphene, where the edge state is flat close to the Fermi level and has a very large effective mass. The effective mass of this one-dimensional edge state can be controlled by electrostatic interactions at the edge of the channel. This result indicates that the mobility of these channels can be controlled by a localized gate voltage. The armchair channel is found to be metallic or semiconducting depending on the width of the channel, in agreement with ribbons and hydrogen-limited channels.

DOI: [10.1103/PhysRevB.83.245424](https://doi.org/10.1103/PhysRevB.83.245424)

PACS number(s): 73.22.Pr, 73.20.At

I. INTRODUCTION

Graphene, a single plane of carbon atoms in a honeycomb lattice, became a fascinating material after the group of Manchester unveiled it from the interior of graphite.¹ Among other intriguing and fascinating properties such as integer quantum Hall effect at room temperature,² graphene exhibits extremely high carrier mobility exceeding 10^7 cm²/(Vs) (Ref. 3) and ballistic transport of carriers on long distances of 10–10² nm (Ref. 4) which make it a promising candidate for future graphene-based field effect transistors. However, the ability to confine carriers and open a gap in graphene is crucial to realize its practical applications. One possibility is to cut narrow stripes in the form of graphene nanoribbons (GNRs). Studies have shown that the GNRs can be made either metallic or semiconducting by controlling their width or orientation.^{5,6} Recent *ab initio* calculations have shown that the electronic structure of the ribbons is not greatly affected by the termination of dangling bonds with hydrogen.^{7,8} These studies have shown that the heavy mass of the edge states in zigzag ribbons induce an instability that creates a localized magnetic moment at the edge.

Two approaches have been attempted to produce GNRs. One method consists of physically cutting the ribbons with either *e*-beam^{9,10} or scanning tunneling microscopy (STM)¹¹ lithography of graphene. However, the reported GNRs by *e*-beam lithography are too wide (15–100 nm) and correspondingly exhibit small band gaps (10–100 meV). Although STM lithography can produce ribbons with smaller widths (2.5–10 nm) and large gaps (0.5–0.18 eV), it requires more time and dexterity. Another approach is to use solution dispersion and sonication^{12,13} to break the graphene into narrow ribbons (sub-10 nm) with varying widths along their lengths. Although this approach can produce many narrow GNRs much easier than the physical cutting approach, it has the disadvantages of much less control of the width of the produced ribbons and type of edge terminations.

Recently, an alternative approach to confine the carriers in graphene has been suggested.¹⁴ The idea is to chemically

modify certain regions of graphene to transform the sp^2 hybridized carbon atoms to sp^3 hybridization. Our group predicted that hydrogenation changes highly conductive graphene into an insulator.¹⁵ The structure of hydrogenated graphene, which we named “graphane,” was previously predicted as stable by Sluiter and Kawazoe.¹⁶ Consequently, hydrogenation can confine the carriers in graphene by sandwiching graphene between two insulating regions. Elias *et al.*¹⁷ hydrogenated graphene and reversibly transformed the material into an insulator, confirming the prediction. Singh *et al.*¹⁸ studied the electronic properties of graphene channels embedded between graphane barriers and found electronic states in the channels that are similar to those of the graphene ribbons. As the channel width is increased row by row, the structures alternate between two cases that are semiconducting and one that is metallic with a total period of three. The zigzag channels possess the peculiar edge state at the Fermi level that corresponds to a one-dimensional electron channel localized at the interface between graphene and graphane with a very flat dispersion relation.^{5,6} Similar to what is observed in the ribbons, the heavy mass of this one-dimensional electronic state induces spin polarization.

Compared to graphane [Ref. 15], graphite fluoride is a material that has been synthesized and studied for many years.^{19–21} Early experimental studies by Parry *et al.*²² and Mahajan *et al.*²³ have measured the structure and electronic properties of (CF)_{*n*} and found that the lattice constants of the hexagonal unit cell are about 2.53 Å in plane and about 5.7 Å in the *c* axis. They also showed (CF)_{*n*} to be an insulator. Charlier *et al.*²⁴ calculated the electronic structure of (CF)_{*n*} and found an insulator with a direct band gap of 3.5 eV at Γ . More recent GW calculations report a much larger band gap of 7.4 eV.^{25,26} Some experimental results have suggested possible routes to remove fluorine atoms and reduce it back to a graphene layer. For instance, the reduction of (CF)_{*n*} and (C₂F)_{*n*} have been attained by hydrogen gas^{27–31} or NaOH-KOH solution.^{32,33} Recent works by Nair *et al.*³⁴ and Robinson *et al.*³⁵ show that fluorinated graphene can be readily patterned and has better stability and insulating properties than hydrogenated graphene.

In this work, we study the electronic properties of graphene channels with zigzag or armchair boundaries limited by insulating graphene fluoride barriers. We will show that the zigzag channels display the peculiar edge state at the Fermi level localized at the interface between graphene and CF, similar to the case of ribbons and channels limited by graphene. However, in the case of the channels limited by CF, the one-dimensional edge state shows a quadratic dispersion relation indicating a smaller effective mass of the carriers. With a simple tight-binding model, we show that the dispersion relation of the peculiar edge state is extremely sensitive to the site energy of the carbon atom at the edge of the graphene channel. The presence of fluorine in the barrier region is responsible for the lower site energy of the carbon atom at the edge and of the dispersion of the edge state. This observation unveils a method to control the dispersion relation of the edge state and consequently the effective mass of the carriers in the channel with a localized gate voltage. Controlling the effective mass with a gate voltage enables switching the spin polarization on and off and modifying the electronic mobility of the structures. The armchair channel is found to be metallic or semiconducting depending on the width of the channel, which is similar to the behavior of armchair ribbons.

II. METHODS

All electronic structure calculations reported in this work were done using density functional theory (DFT) with a plane-wave basis set as implemented in the Vienna *Ab Initio* Simulation Package (VASP).^{36–39} The core electrons were treated with a frozen projector augmented-wave method.^{40,41} The exchange and correlation potential was treated with a generalized gradient approximation using the Perdew-Burke-Ernzerhof (PBE) functional.^{42,43} The plane-wave energy cutoff determining the basis set size was set to 400 eV, and the Brillouin zone was sampled with a Monkhorst-Pack⁴⁴ grid of $8 \times 1 \times 1$ (for zigzag) and $1 \times 8 \times 1$ (for armchair). For the density-of-states calculation we use a k -point sampling of $64 \times 16 \times 1$ (for zigzag) and $16 \times 64 \times 1$ (for armchair). A vacuum of 12 Å is added in the direction normal to the GR/CF superlattice plane to avoid artificial interactions of the images. For the relaxed configurations in this work, the converged atomic forces were smaller than 0.01 eV/Å.

We have tested the above calculation setup for graphene fluoride, which shows a band gap of 3.1 eV at the Γ point and lattice constant of the hexagonal unit cell at 2.61 Å. The lattice constant is in good agreement with the neutron-scattering value of 2.61 Å recently obtained by Sato.²⁰ The lattice constant of the superlattices is approximated by a linear interpolation between the lattice constant of graphene and CF. The lattice constant of a structure of M rows of CF (the barrier) and N rows of graphene (the channel) is calculated as

$$a_{\text{GR/GF}} = \frac{M}{M+N} a_{\text{GF}} + \frac{N}{M+N} a_{\text{GR}}, \quad (1)$$

where $a_{\text{GF}} = 2.61$ Å and $a_{\text{GR}} = 2.46$ Å. None of the results presented in this work are strongly dependent on the small departures from this approximation. All the structures

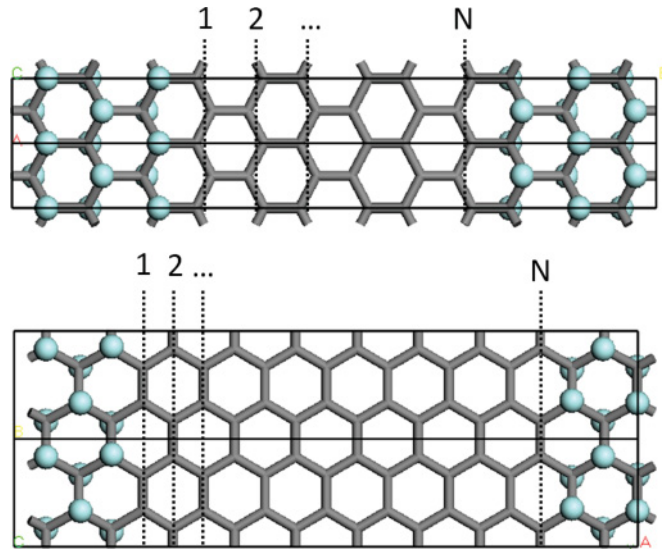


FIG. 1. (Color online) Zigzag (top) and armchair (bottom) channels of graphene limited by a barrier region of graphene fluoride. The carbon network is represented in gray while the fluorine atoms are represented by light blue balls. For each geometry we indicate the convention to count the number of rows in the channel; this is generically called N in the text. The number of rows in the barrier region is generically called M and counted in the same way. For clarity, two unit cells are presented in each case.

considered have been optimized with respect to the atomic positions. Two representative examples are shown in Fig. 1. In the rest of this paper, we will use a notation $zz(M,N)$ or $ac(M,N)$ depending on whether the orientation is zigzag or armchair, respectively, to refer to structures with M rows of carbon atoms in the barrier and N rows of carbon atoms in the channel. This nomenclature is graphically indicated in Fig. 1.

III. RESULTS AND DISCUSSION

Zigzag channels. The electronic structure of the zigzag channels shares its general features with their analog channels limited by graphene or with the ribbons. The features we will describe can be understood with a tight-binding model with one p_z orbital per atom and hopping to first neighbors in the channel.^{5,6} In Fig. 2 we show the bands close to the Fermi level of a $zz(6,12)$ channel. They have two degenerate states at the Fermi level in the X point of the Brillouin zone that disperse along the X - Γ direction, which is the direction corresponding to motion along the channel, forming two bands that will be the center of our discussion below. In a zigzag structure with N rows of carbon atoms in the channel, there are other $2N-2$ bands derived from the folding of the π and π^* bands of graphene divided in two manifolds of $N-1$ bands each, one above and one below the Fermi level. Each of these manifolds is almost degenerate at the X point at an energy approximately equal to the first-neighbors hopping of the p_z orbitals above and below the Fermi level. Due to the dispersion in the direction X - Γ , these states form a gap at about 1/3 of the distance from the X point to the Γ point. This gap gets smaller as the channel gets wider. This intermediate point 1/3 of the distance from

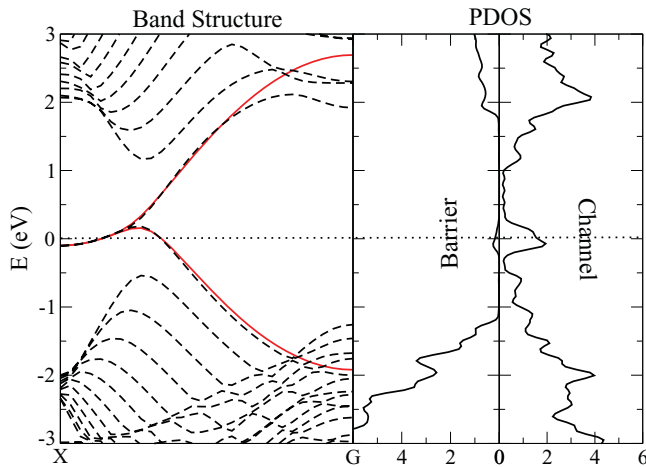


FIG. 2. (Color online) Band structure on the left and partial density of states of the barrier and channel region of a zigzag structure $zz(6,12)$. The tight-binding approximation of the edge state around the Fermi level is shown with a continuous line in red. The tight-binding model demonstrates that the dispersion relation of the edge state is controlled by the site energy of the carbon atoms at the edge.

the X point, which is the folded location of the K point in the graphene band structure, is also important for the states at the Fermi level. They disperse together up to this point when one of them moves up in energy and the other moves down away from the Fermi level to almost join the manifolds at the Γ point. The charge density associated with these states is mainly localized at the edge. It is strictly localized at the edge row for the states at X and the localization length increases as the states depart from this point. The features described are also evident from the partial density of states at the barrier and at the channel region, also shown in the right panel of Fig. 2. The barrier shows a big gap except for a small contribution from the edge state at the Fermi level. The density of states of the channels at the Fermi level is dominated by the edge states and the manifolds appear around it. They are still in the gap regions of the barrier indicating their localization.

In channels limited by graphane and in ribbons these two states remain pinned to the Fermi level until they separate at about the intermediate point $1/3$ of the distance from the X point. For a semi-infinite plane, they will separate exactly with no gap between the manifolds at this point. However, in the channels limited by CF these two states disperse together quadratically up to this point before separating to join the manifolds. This quadratic dispersion signifies that the carriers in the channels will have a smaller effective mass with all its implications to mobility. Understanding the origin of this peculiar behavior will enable control of the effective mass of this one-dimensional channel with interesting implications for applications.

The origin of the dispersion of the edge state must be a property of CF affecting the interface. One important property is the large electron affinity of CF. Since fluorine is the most electronegative element of the periodic table there is an important charge transfer from the middle carbon layer to the external fluorine layers. From an electrostatic point of view,

the system can be represented by two negative layers outside a central positively charged layer. All carbon atoms are sitting at a much lower potential than the vacuum level, much lower than, for example, in graphane. This results in a very large electron affinity. We have estimated the electron affinity of CF as the difference between the vacuum level of the electrostatic potential and the bottom of the conduction band to be 4.8 eV. This value is lower than the work function of graphene that we estimate (using the same method) to be 4.6 eV. This means that there will be an interface dipole formed at the junction between graphene and CF, and the edge atoms of the channel will be sitting at a lower potential energy with respect to the center of the channel. To prove this hypothesis, we modified the tight-binding model used to describe the ribbons^{5,6} adding a term that lowers the site energy of the carbon p_z orbital at the edge with respect to the site energy of similar orbitals in the center of the channel. This simple modification indeed produces the desired effect. The resulting tight-binding band is plotted with a continuous line, as shown in Fig. 2. The figure shows excellent agreement except for a slight deviation close to the Γ point where this band starts mixing more with other bands not considered in the simplified tight-binding model. This agreement was obtained for a site energy at the edge that is 0.5 eV lower with respect to the other orbitals and a hopping integral equal to 2.3 eV. This confirms that the lowering of the site energy at the edge is a reasonable explanation for the dispersion relation of the edge states.

The agreement shown in Fig. 2 corresponds to a $zz(6,12)$ structure. We found that all the structures we explored with channel widths from 8 to 12 can be fitted with the same excellent agreement using the same parameters for hopping and edge site energy. These fitting parameters are also a good value for different barrier widths. These results confirm the expectation that we are describing an effect whose origin is well localized at the interface and not affected by the presence of the other edge. It is possible that for very narrow channels both edge states influence each other. However, this is of no practical importance.

As a result of the lower site energy of the edge carbon atom, an evaluation of the charge distribution with the tight-binding model results in 5% more electrons occupying the edge orbital with respect to the orbitals at the center of the channel. This result is in good agreement with similar estimations with the DFT calculations.

Armchair channels. As the number of rows in the armchair channels increases, their electronic structure around the Fermi level goes in a cycle of period three with two semiconducting and one almost-semimetallic case. This feature has been reported previously⁴⁵ and is shared by the ribbons with^{5,6} and without^{7,8} hydrogen termination and with the channels limited by graphane.¹⁸ The results of our calculations are summarized in Fig. 3 where the electronic band gap at the Fermi level is plotted as a function of the channel width for different widths of the barrier. The figure shows that the band gaps are almost independent of the size of the barrier region for the rather small sizes represented here. As expected, this dependence will disappear as the size of the barrier becomes large. The figure also shows that the band gap obtained for each period decreases as the channel width increases due to a reduction of the quantum confinement for

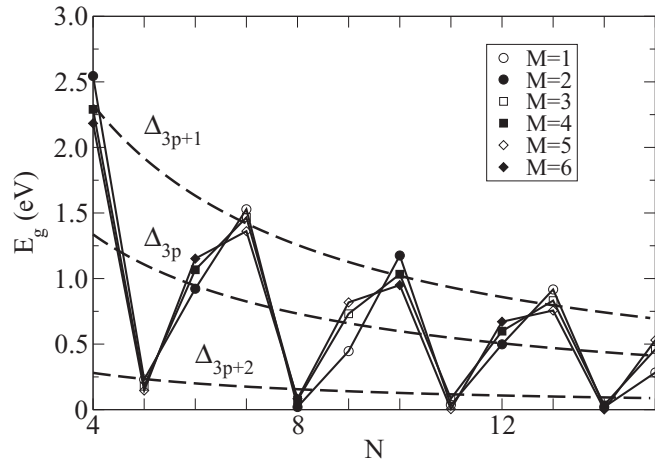


FIG. 3. Band gap of armchair channels as a function of the number of rows in the channel N , for a different number of rows in the barrier, M . The dashed lines correspond to the tight-binding approximation with hopping integral equal to 2.6 eV and a 9% increase of the hopping at the edge.

wider channels. Let $E_g(M, N)$ represent the gap, obtained by DFT, of a structure with M rows in the barrier and N rows in the channel. The armchair channels can be divided into three classes corresponding to N equal to $3p$, $3p + 1$, and $3p + 2$ for any natural number p . The band gap follows the hierarchy $E_g(M, 3p + 1) > E_g(M, 3p) > E_g(M, 3p + 2)$. The $3p$ and $3p + 1$ classes are semiconducting, while the $3p + 2$ class is almost semimetallic with a band gap on the order of a few millielectron volts.

This hierarchy is different than the result expected from a tight-binding model with uniform hopping integrals and similar to the hierarchy obtained for hydrogenated ribbons by Son, Cohen, and Louie.⁸ These authors provided an interesting analysis of the origin of this discrepancy that can be explained assuming a different hopping between the carbon atoms at the edge of the ribbon. They found expressions for the gaps of the different classes to first order in the hopping perturbation. Their results for these gaps, Δ_{3p} , Δ_{3p+1} , and Δ_{3p+2} are provided in Eq. (1) of their paper. The DFT results in their case can be reproduced if they assume a hopping integral in ribbon $t = 2.7$ eV except at the edge where the hopping integral is 12% larger. We notice that, contrary to this observation, Muñoz and co-workers⁴⁵ obtain a different hierarchy for the gaps. In view of the tight-binding model, this difference can be related to the hopping integral at the edge and possibly to the difference in the relaxation geometry.

As can be seen in Fig. 3, although there is some variation in each class due to the different barrier widths considered, our results for the channels limited by CF barriers can also be described by the same model. We can reproduce the behavior of our DFT results assuming a hopping integral $t = 2.6$ eV except for the edge carbon atoms where the hopping integral is 9% larger. The beauty of these expressions is that it permits a correct extrapolation to larger channel widths, not accessible to DFT calculations but easier to realize experimentally. This extrapolation to a large channel width, W_a , is $\Delta_i \rightarrow a_i W_a^{-1}$. It

behaves as expected, scaling as the inverse of the width with a coefficient for each class given by

$$\begin{aligned} a_{3p} &= ta(\pi - \delta 6\sqrt{3}) \approx 0.81 \text{ eV nm}, \\ a_{3p+1} &= ta(\pi + \delta 3\sqrt{3}) \approx 1.33 \text{ eV nm}, \\ a_{3p+2} &= ta\delta 3\sqrt{3} \approx 0.17 \text{ eV nm}, \end{aligned} \quad (2)$$

where $a = 0.142$ nm is the distance between carbon atoms in graphene.

In addition to the interesting behavior of the gap, the electronic states close to the Fermi level are localized in the channel. Figure 4 shows two typical band structures for armchair channels. The top panel corresponds to a semiconducting channel, ac(5,13) with a width of 15 Å and the lower panel to a semimetallic one, ac(6,14) with a width of 16 Å. On the right of the band structure we show the partial density of states projected on the barrier region and on the channel region. The localization is apparent from these plots. In both cases the barrier region displays a band gap of the order of

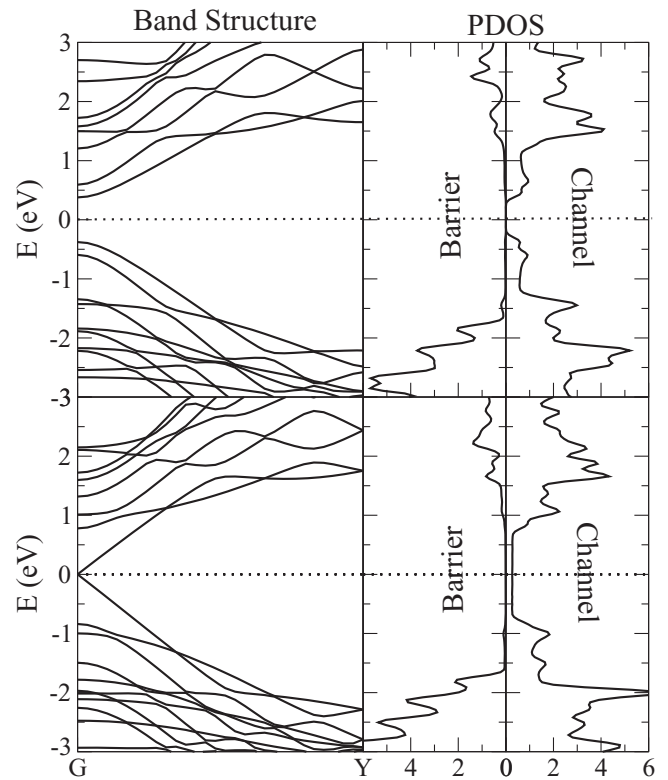


FIG. 4. Band structure and partial density of states in the barrier and channel region of two representative armchair channels. The top panel corresponds to a semiconducting channel, ac(5,13), and the bottom panel to a semimetallic channel, ac(6,14). From the band structure in the top panel, we see that the semiconducting armchair channel has a direct gap. From the density of states we see that the states close to the gap are localized within the channel because the gap in the channel is centered with respect to the gap in the barrier. For the band structure in the bottom panel we see that the semimetallic structures have a one-dimensional linear band, localized within the channel and producing a constant density of states.

3 eV, characteristic of graphene fluoride. In the case of the semiconducting channel, the top of the valence band and the bottom of the conduction band in the channel region are well localized in the middle of the barrier gap. The small gap of the channel is well aligned in the center of the larger gap in the barrier. This indicates that both electrons and holes will be localized within the channel.

The case of the semimetallic channel, displayed in the bottom panel of Fig. 4, is also very interesting. The one-dimensional bands close to the Fermi level have a linear dispersion relation along the direction of the channel. These bands produce a constant density of states around the Fermi level as can be seen from the partial density of states in the channel region.

It is not surprising that the electronic structure around the Fermi level is not different for channels limited by CF compared to that of channels limited by graphane or ribbons. The CF barriers have a large effect on the edge sites as demonstrated for the zigzag ribbons. The armchair channels as well as the ribbons do not have edge states. All states around the Fermi level are confined in the channel and the corresponding wave functions have very low weight at the edge sites. Therefore, the wave functions are less affected by changes in these sites.

IV. CONCLUSIONS

In summary, we presented DFT calculations of the electronic structure of zigzag and armchair channels embedded in a matrix of graphene fluoride. The results are analyzed with a tight-binding model of the carbon p_z orbitals in the channel. The zigzag channels and ribbons always show an edge state at the Fermi level that corresponds to a one-dimensional electronic state that moves along the edge of the channel. The dispersion relation of this state, along the $X-\Gamma$ direction determines the effective mass of this carrier. In channels limited by graphane or in ribbons, the effective mass of this carrier is very high; the state shows a flat band at the Fermi level. For the channels limited by graphene fluoride, this band shows a quadratic dispersion indicating a lower effective mass of carriers. A tight-binding analysis indicates that the quadratic dispersion can be explained by a lower site energy of the carbon atoms' p_z orbitals at the edge of the channel. We argue that this effect is caused by the large electron affinity of CF that produces an interfacial dipole moment and lowers the electrostatic potential in this region. The extra charge accumulated in response by this change in the electrostatic potential is observed in the DFT calculations and is in good agreement with the results of the tight-binding model. It is important to notice that these results are independent of the exact value of the band gap of the barrier region, a quantity that it is so far unknown with theoretical values ranging from 3.1 eV using DFT/GGA (generalized gradient approximation)²⁴ to 7.4 eV using GW.^{25,26} As long as the CF region produces a negative electrostatic potential on the carbon plane, the carbon atoms at the edge will be more attractive to electrons and, as demonstrated in our work, will add dispersion to the edge states.

This observation suggests a method to control the effective mass of carriers in the channel by modifying the electrostatic

potential around the edge. This can be done by a localized knife-shaped gate potential⁴⁶ or by the selective absorption of ferroelectric polymers such as polyvinylfluoride⁴⁷ that are chemically compatible with graphene fluoride. The change in the effective mass of the carriers close to the Fermi level will induce a change in the mobility⁴⁸ and in the magnetic properties of the channels.⁴⁹ It is interesting to notice that the formation of a magnetic moment on the edge atoms of the ribbons is a consequence of a competition between the intrasite Coulomb repulsion in the p_z orbitals and the hopping between edge sites. A smaller effective mass of the edge states corresponds to a larger hopping probability between edge sites. This larger hopping may overcome the Coulomb-induced localization and remove the localized magnetization. Our group is currently working on these possibilities.

The armchair channels are less affected by the materials that provide the confinement and the graphene fluoride-embedded structures have similar electronic structures to those of the graphane-embedded structures or the ribbons. This is expected because, in the absence of edge states, all states in the channel have very low weight of their wave function on the carbon atoms close to the edge. A tight-binding analysis shows that the main effect at the interface is given by a 9% increase of the hopping integral between carbon atoms at the edge. This assumption explains the scaling and relative values of band gaps for different widths of the channels. The one-dimensional bands observed in the armchair channels of the $3p+2$ class derive from the Dirac points of the graphene band structure and possess very interesting symmetry properties.

The experimental realization of these structures has already been attempted in many labs,^{31,35,50} and their stability depends on the diffusion of fluorine on graphene. Our current estimate for the diffusion barrier of an isolated fluorine atom on graphene is of the order of 0.3 eV. Assuming a standard attempt jump frequency of 10^{13} 1/s, this barrier implies a diffusion coefficient of 2×10^8 nm²/s at 300 K. However, if the fluorine atom is close to other fluorine atoms on the surface of graphene, the barrier for diffusion is of the order of 1 eV, and the diffusion coefficient is as low as 3×10^4 nm²/s at the same temperature. These diffusion barriers have been estimated with the nudged elastic band method^{51,52} with the same setup used for all other VASP calculations in this paper. A similar result was recently reported for the case of hydrogen on graphene.⁵³ Ao and co-workers report that the barrier for hydrogen diffusion on graphene is almost ten times larger when the hydrogen atoms are at the armchair or zigzag interfaces. These results seem to indicate that, although isolated fluorine atoms will diffuse quite fast on the surface, once assembled in the region of the barrier, the structure will be stable at room temperature.

ACKNOWLEDGMENTS

This work was supported by NSF MRSEC Grant No. DMR-0820404 and by the Donors of the American Chemical Society Petroleum Research Fund. The authors acknowledge the use of facilities at the NSF NNIN and the Penn State Materials Simulation Center.

*sofo@psu.edu

- ¹K. S. Novoselov, A. K. Geim, S. V. Morozov, D. Jiang, Y. Zhang, S. V. Dubonos, I. V. Grigorieva, and A. A. Firsov, *Science* **306**, 666 (2004).
- ²K. S. Novoselov, Z. Jiang, Y. Zhang, S. V. Morozov, H. L. Stormer, U. Zeitler, J. C. Maan, G. S. Boebinger, P. Kim, and A. K. Geim, *Science* **315**, 1379 (2007).
- ³P. Neugebauer, M. Orlita, C. Faugeras, A. L. Barra, and M. Potemski, *Phys. Rev. Lett.* **103**, 136403 (2009).
- ⁴W. K. Tse, E. H. Hwang, and S. D. Sarma, *Appl. Phys. Lett.* **93**, 023128 (2008).
- ⁵K. Nakada, M. Fujita, G. Dresselhaus, and M. S. Dresselhaus, *Phys. Rev. B* **54**, 17954 (1996).
- ⁶M. Fujita, K. Wakabayashi, K. Nakada, and K. Kusakabe, *J. Phys. Soc. Jpn.* **65**, 1920 (1996).
- ⁷Y. W. Son, M. L. Cohen, and S. G. Louie, *Nature (London)* **444**, 347 (2006).
- ⁸Y. W. Son, M. L. Cohen, and S. G. Louie, *Phys. Rev. Lett.* **97**, 216803 (2006).
- ⁹M. Y. Han, B. Ozyilmaz, Y. B. Zhang, and P. Kim, *Phys. Rev. Lett.* **98**, 206805 (2007).
- ¹⁰Z. H. Chen, Y. M. Lin, M. J. Rooks, and P. Avouris, *Physica E* **40**, 228 (2007).
- ¹¹L. Tapasztó, G. Dobrik, P. Lambin, and L. P. Biro, *Nat. Nanotechnol.* **3**, 397 (2008).
- ¹²X. L. Li, X. R. Wang, L. Zhang, S. W. Lee, and H. J. Dai, *Science* **319**, 1229 (2008).
- ¹³X. R. Wang, Y. J. Ouyang, X. L. Li, H. L. Wang, J. Guo, and H. J. Dai, *Phys. Rev. Lett.* **100**, 206803 (2008).
- ¹⁴R. Ruoff, *Nat. Nanotechnol.* **3**, 10 (2008).
- ¹⁵J. O. Sofo, A. S. Chaudhari, and G. D. Barber, *Phys. Rev. B* **75**, 153401 (2007).
- ¹⁶M. H. F. Sluiter and Y. Kawazoe, *Phys. Rev. B* **68**, 085410 (2003).
- ¹⁷D. C. Elias, R. R. Nair, T. M. G. Mohiuddin, S. V. Morozov, P. Blake, M. P. Halsall, A. C. Ferrari, D. W. Boukhvalov, M. I. Katsnelson, A. K. Geim, and K. S. Novoselov, *Science* **323**, 610 (2009).
- ¹⁸A. K. Singh and B. I. Yakobson, *Nano Lett.* **9**, 1540 (2009).
- ¹⁹H. Touhara, J. Inahara, T. Mizuno, Y. Yokoyama, S. Okanao, K. Yanagiuchi, I. Mukopadhyaya, S. Kawasakia, F. Okino, H. Shiraic, W. H. Xud, T. Kyotanid, and A. Tomita, *J. Fluorine Chem.* **114**, 181 (2002).
- ²⁰Y. Sato, K. Itoh, R. Hagiwara, T. Fukunaga, and Y. Ito, *Carbon* **42**, 2897 (2004).
- ²¹H. Touhara and F. Okino, *Carbon* **38**, 241 (2000).
- ²²D. E. Parry, J. M. Thomas, B. Bach, and E. L. Evans, *Chem. Phys. Lett.* **29**, 128 (1974).
- ²³V. K. Mahajan, Rb Badachha., and J. L. Margrave, *Inorg. Nucl. Chem. Lett.* **10**, 1103 (1974).
- ²⁴J. C. Charlier, X. Gonze, and J. P. Michenaud, *Phys. Rev. B* **47**, 16162 (1993).
- ²⁵M. Klintonberg, S. Lebègue, M. I. Katsnelson, and O. Eriksson, *Phys. Rev. B* **81**, 085433 (2010).
- ²⁶O. Leenaerts, H. Peelaers, A. D. Hernández-Nieves, B. Partoens, and F. M. Peeters, *Phys. Rev. B* **82**, 195436 (2010).
- ²⁷Y. Sato, R. Hagiwara, and Y. Ito, *J. Fluorine Chem.* **110**, 31 (2001).
- ²⁸Y. Sato, H. Watano, R. Hagiwara, and Y. Ito, *Carbon* **44**, 664 (2006).
- ²⁹Y. Sato, S. Shiraishi, H. Watano, R. Hagiwara, and Y. Ito, *Carbon* **41**, 1149 (2003).
- ³⁰N. Kumagai, M. Kawamura, H. Hirohata, K. Tanno, Y. Chong, and N. Watanabe, *J. Appl. Electrochem.* **25**, 869 (1995).
- ³¹S. H. Cheng, K. Zou, F. Okino, H. R. Gutierrez, A. Gupta, N. Shen, P. C. Eklund, J. O. Sofo, and J. Zhu, *Phys. Rev. B* **81**, 205435 (2010).
- ³²A. B. Bourlinos, V. Georgakilas, R. Zboril, D. Jancik, M. A. Karakassides, A. Stassinopoulos, D. Anglos, and E. P. Giannelis, *J. Fluorine Chem.* **129**, 720 (2008).
- ³³J. Giraudet, M. Dubois, J. Inacio, and A. Hamwi, *Carbon* **41**, 453 (2003).
- ³⁴W. C. R. R. Nair, R. Jalil, I. Riaz, V. G. Kravets, L. Britnell, P. Blake, F. Schedin, A. S. Mayorov, S. Yuan, M. I. Katsnelson, H. M. Cheng, W. Strupinski, L. G. Bulusheva, A. V. Okotrub, K. S. Novoselov, A. K. Geim, I. V. Grigorieva, and A. N. Grigorenko, *Small* **6**, 2877 (2010).
- ³⁵J. T. Robinson, J. S. Burgess, C. E. Junkermeier, S. C. Badescu, T. L. Reinecke, F. K. Perkins, M. K. Zalalutdniov, J. W. Baldwin, J. C. Culbertson, P. E. Sheehan, and E. S. Snow, *Nano Letter.* **10**, 3001 (2010).
- ³⁶G. Kresse and J. Hafner, *Phys. Rev. B* **47**, 558 (1993).
- ³⁷G. Kresse and J. Hafner, *J. Phys.: Condens. Matter.* **6**, 8245 (1994).
- ³⁸G. Kresse and J. Furthmüller, *Phys. Rev. B* **54**, 11169 (1996).
- ³⁹G. Kresse and J. Furthmüller, *Comput. Mater. Sci.* **6**, 15 (1996).
- ⁴⁰P. E. Blöchl, *Phys. Rev. B* **50**, 17953 (1994).
- ⁴¹G. Kresse and D. Joubert, *Phys. Rev. B* **59**, 1758 (1999).
- ⁴²J. P. Perdew, K. Burke, and M. Ernzerhof, *Phys. Rev. Lett.* **77**, 3865 (1996).
- ⁴³J. P. Perdew, K. Burke, and M. Ernzerhof, *Phys. Rev. Lett.* **78**, 1396 (1997).
- ⁴⁴H. J. Monkhorst and J. D. Pack, *Phys. Rev. B* **13**, 5188 (1976).
- ⁴⁵E. Muñoz, A. K. Singh, M. A. Ribas, E. S. Penev, and B. I. Yakobson, *Diamond Relat. Mater.* **19**, 368 (2010).
- ⁴⁶S. Woo and Y. W. Son, in [<http://meetings.aps.org/link/BAPS.2010.MAR.W22.4>].
- ⁴⁷Y.-L. Lee, S. Kim, C. Park, J. Ihm, and Y.-W. Son, *ACS Nano* **4**, 1345 (2010).
- ⁴⁸M. Q. Long, L. Tang, and D. Wang, *J. Am. Chem. Soc.* **131**, 17728 (2009).
- ⁴⁹L. Pisani, J. A. Chan, B. Montanari, and N. M. Harrison, *Phys. Rev. B* **75**, 064418 (2007).
- ⁵⁰M. Baraket, S. G. Walton, E. H. Lock, J. T. Robinson, and F. K. Perkins, *Appl. Phys. Lett.* **96**, 231501 (2010).
- ⁵¹G. Henkelman and H. Jonsson, *J. Chem. Phys.* **113**, 9978 (2000).
- ⁵²D. Sheppard, R. Terrell, and G. Henkelman, *J. Chem. Phys.* **128**, 134106 (2008).
- ⁵³Z. M. Ao, A. D. Hernández-Nieves, F. M. Peeters, and S. Li, *Appl. Phys. Lett.* **97**, 233109 (2010).